RSC Advances

PAPER

View Article Online
View Journal | View Issue

Cite this: *RSC Adv.*, 2018, **8**, 18745

Zein regulating apatite mineralization, degradability, *in vitro* cells responses and *in vivo* osteogenesis of 3D-printed scaffold of n-MS/ZN/PCL ternary composite

Jiangying Ru,[a] Qiang Wei,[b] Lianqing Yang,[b] Jing Qin,[c] Liangchen Tang,[c] Jie Wei,[c] Lieping Guo*[d] and Yunfei Niu*[b]

Bioactive and degradable scaffolds of nano magnesium silicate (n-MS)/zein (ZN)/poly(caprolactone) (PCL) ternary composites were prepared by 3D-printing method. The results showed that the 3D-printed scaffolds possessed controllable pore structure, and pore morphology, pore size, porosity and pore interconnectivity of the scaffolds can be efficiently adjusted. In addition, the apatite-mineralization ability of the scaffolds in simulated body fluids was obviously improved with the increase of ZN content, in which the scaffold with 20 w% ZN (C20) possessed excellent apatite-mineralization ability. Moreover, the degradability of the scaffolds was significantly enhanced with the increase of ZN content in the scaffolds. The degradation of ZN produced acidic products that could neutralize the alkaline products from the degradation of n-MS, which avoid the increase of pH value in degradable solution. Furthermore, the MC3T3-E1 cells responses (*e.g.* proliferation and differentiation, *etc.*) to the scaffolds were significantly promoted with the increase of ZN content. The *in vivo* osteogenesis of the scaffolds implanted the femur defects of rabbits was investigated by micro-CT and histological analysis. The results demonstrated that the new bone formation was significantly enhanced with the increase of ZN content, in which the C20 scaffold induced the highest new bone tissues, indicating excellent osteogenesis. The results suggested that the ZN in the ternary composite scaffolds played key roles in assisting bone regeneration *in vivo*.

Received 26th March 2018
Accepted 9th May 2018

DOI: 10.1039/c8ra02595a

rsc.li/rsc-advances

Introduction

Over the past few decades, bioactive scaffolds of polymer based biocomposites containing bioactive materials (*e.g.* hydroxyapatite, tricalcium phosphate, bioglass, and calcium silicate, *etc.*) and degradable polymers (*e.g.* poly(lactic acid), poly(glycolic acid), poly(lactic-*co*-glycolic acid) and poly(caprolactone), *etc.*) with great potential for tissue engineering scaffolds have been widely reported.[1–3] The polymer based biocomposites scaffolds have been fabricated by means of different conventional technologies, including rapid prototyping, solvent casting and particulate-leaching, gas foaming, foam replica method, electrospinning, freeze-drying and phase separation, *etc.*[4–6] The advantages of these conventional methods are inexpensive and simple, which are flexible to optimize or control physical–chemical and biological performances of the scaffolds. However, the main disadvantages of these technologies are that they cannot efficiently modulate the porous structures of the scaffolds, such as pore size, porosity, pore morphology, and pore interconnectivity, *etc.*[7]

Synthetic polymer of biodegradable poly(caprolactone) (PCL) with good biocompatibility and mechanical strengths has been applied in biomedical fields for many years.[8] However, the significant disadvantages of PCL are that PCL is bioinert materials (no inducing new bone regeneration) and its degradability is very slow both *in vitro* and *in vivo*.[9] Natural polymer of plant proteins (*e.g.* zein, soy proteins and wheat protein, *etc.*) have attracted more and more interests for biomedical materials.[10] Due to the excellent biocompatibility and biodegradability, biomaterials developed from plant proteins are preferred for biomedical applications over synthetic polymers.[11] One of plant proteins of zein (ZN) with good biocompatibility have been investigated for various applications, such as deoxyribonucleic acid (DNA) transfection, vaccine delivery, oral delivery of proteins and peptides, and tissue engineering scaffolds.[12,13] The advantage of ZN is its fast

[a]*Department of Orthopaedics, The Affiliated Hospital of Yangzhou University, Yangzhou University, Yangzhou 225009, China*
[b]*Department of Orthopaedics, Changhai Hospital, Second Military Medical University, Shanghai 200433, China. E-mail: niuyunfei1219@163.com*
[c]*Key Laboratory for Ultrafine Materials of Ministry of Education, East China University of Science and Technology, Shanghai 200237, China*
[d]*Department of Oncology, Shanghai Eastern Hepatobiliary Surgery Hospital, Shanghai, 200438, China. E-mail: glplaying2000@163.com*

biodegradability while the disadvantage of ZN is its low mechanical strength.[12–14]

Previous study reported that nano magnesium silicate (n-MS) bioglass exhibited superior *in vitro* bioactivity (apatite formation), cytocompatibility and *in vivo* osteogenesis properties as compared with traditional magnesium silicate bioglass.[15,16] However, the main disadvantages of n-MS are its inherent brittleness and low mechanical strength.[15,16] Combination of the advantages of both biodegradable polymers and bioactive materials would cause the composites scaffolds with improved bioperformances (*e.g.* bioactivity, degradability and mechanical strength, *etc.*).[17]

Recently, the scaffolds fabricated by 3D-printing have been utilized for application in bone tissue engineering.[18] The significant advantages of this method are that the porous structures (pore morphology, pore size, porosity and interconnectivity, *etc.*) of the scaffolds can be concisely controlled by layer-by-layer plotting under different conditions.[18,19] Therefore, in this study, nano magnesium silicate (n-MS) particles were fabricated, and bioactive and degradable scaffolds of n-MS/ZN/PCL ternary composites with controllable pore structure were developed by 3D printing method. The objective of this study to investigate the effects of ZN content in the scaffolds on *in vitro* apatite mineralization, degradability, cell responses and *in vivo* osteogenesis properties of the ternary composites scaffolds.

Materials and methods

Preparation and characterization of nano magnesium silicate

The nano magnesium silicate (n-MS) were synthesized by a sol–gel method using cetyltrimethylammonium bromide (CTAB) as the template, in which 6.6 g CTAB was firstly dissolved in 600 mL distilled water, then 12 mL ammonia aqueous solution (28 w%) was added into the CTAB solution. After stirring for 1 h, 30 mL tetraethyl orthosilicate (TEOS, 98%) and 17.2 g $Mg(NO_3)_2 \cdot 6H_2O$ were added into the solution and stirred for 6 h. The products were collected by vacuum filtration, and washed by distilled water and ethanol for 3 times, respectively, then dried at 60 °C for 24 h. The resulting powders were then calcined at 550 °C for 2 h to remove the CTAB, and the final n-MS powders were obtained.[15,16] All raw materials used in this process were purchased from Shanghai Lingfeng Chemical Reagent Co., Ltd., China. The n-MS powders were characterized by transmission electron microscopy (TEM, 2100F, JEOL, Japan), EDS (TEM, 2100F, JEOL, Japan) and X-ray diffraction (XRD, D/Max 2550V, Rigaku, Japan).

Preparation and characterization of ternary composites scaffolds

The 3D Bioplotter™ printing device (EnvisionTEC GmbH, Germany) was used to prepare 3D-printed scaffolds. Prior to printing the scaffolds, the injectable n-MS/ZN/PCL paste was prepared as following: 2 g mixture containing n-MS, ZN and PCL was dispersed into 20 mL chloroform according to the component proportion listed in Table 1. The dispersion was then quickly stirred at room temperature until it formed a paste for injection. Finally, the prepared paste was introduced into a polyethylene injection cartridge, which was fixed onto the device. Simultaneously, square block models (6 × 6 × 6 mm) were loaded on the Bioplotter™ CAD/CAM software, and the scaffolds were plotted layer-by-layer through the extrusion of the paste. The architecture was changed by plotting fibers with 0 and 90 angle steps between two successive layers; the dosing pressure to the syringe pump was 1.5–3.0 bar, the speed of the dispensing unit was 1.5–5 mm s^{-1}, and the nozzle size was 0.25 mm. Finally, the obtained n-MS/ZN/PCL scaffolds (C0, C10, C20) were dried in an oven at 37 °C for 2 days (evaporate chloroform).

Table 1 Composition of scaffolds prepared by 3D printing method

Samples	C0	C10	C20
ZN	0	10 w%	20 w%
PCL	70 w%	60 w%	50 w%
n-MS	30 w%	30 w%	30 w%

The as-prepared scaffolds were characterized by scanning electron microscope (SEM, S-4800, Hitachi, Japan) and XRD. The porosity of the 3D-printed scaffolds was evaluated by using Archimedes method: porosity $= (W_b - W_a)/(W_b - W_c) \times 100\%$, where W_a was the dry weight of the samples, W_b was the wet weight of the scaffolds and W_c was the weight of the scaffolds suspended in water. The compressive strength of the 3D-printed scaffolds was evaluated by using a mechanical testing machine (HY-0230, Shanghai, China).

Apatite mineralization of scaffolds in SBF

The assessment of *in vitro* bioactivity of the scaffolds was carried out in simulated body fluids (SBF) solution. Each scaffold was soaked in 10 mL of SBF solution in a polyethylene bottle at 37 °C for different time. At each time interval, the scaffolds were collected, washed gently with distilled water, and dried at 60 °C. SEM and EDS were used to examine the mineralized apatite on scaffolds surfaces. The ions concentrations (Mg, Si, Ca and P) in solution after the scaffolds soaking for different time were determined by ICP-AES (Perkin-Elmer Optima 7000DV).

Degradation of scaffolds in PBS

To evaluation the degradable properties of the scaffolds, the weight change of the samples before and after soaking into phosphate buffer saline (PBS) for up to 84 days was monitored by the electronic analytical balance (AL204, Mettler Toledo, Switzerland), and the weight change ratio was calculated according to the following equation:[18] weight change (%) $= (W_n - W_0)/W_0$, where W_0 represents the samples weight before soaking and W_n represents samples weight after soaking for different times. In addition, the change of pH value in solution for the scaffolds during the immersion period was also measured by a pH meter (FE20K, Mettler Toledo, Switzerland) at designated points of time.

In vitro cytocompatibility of scaffolds

Cells culture. MC3T3-E1 cells, an osteoblast precursor cell line derived from mouse (Cell Culture Center, Chinese Academy of Medical Science, China), was used to evaluate influence of the scaffolds on cell proliferation and differentiation. The cells were cultured in Dulbecco's Modified Eagle Medium (DMEM, Gibco, USA) supplemented with 10% fetal bovine serum (FBS, Gibco, ThermoFisher Scientific, USA), 100 U mL^{-1} penicillin and 100 μg mL^{-1} streptomycin sulphate at 37 °C in a humidified atmosphere of 5% CO_2. Then the cells were detached with 0.25% trypsin, 0.03% ethylene diamine tetraacetic acid (EDTA) and the cell density was counted. After counting, the cell suspension was diluted to the desired density for following cell experiments. After sterilized by ethylene oxide, the scaffolds were placed into 24-well plate and co-cultured with the cells with density of 1×10^5 cells per well for different time.

Cells morphology and proliferation. After culturing for 6 h, the scaffolds with the cells were fixed in 4% paraformaldehyde for 30 min, and rinsed with phosphate-buffered saline (PBS) for 3 times. Moreover, the samples were treated with 0.1% Triton X-100 to permeabilize the cells for 20 min and then blocked with 1% BSA for 20 min. Finally, the actin cytoskeletons were labeled by incubating with Phalloidin-FITC (Sigma, USA) for 30 min, and the cell nuclei were contrast-labeled in blue by 4′6-diamidino-2-phenylindole dihydrochloride (DAPI, Sigma, USA) for 5 min. The actin cytoskeletons of cells were visualized with a confocal laser scanning microscope (CLSM, Leica, Germany).

For the cell proliferation assay, the cells were cultured on the samples in 24-well plates for 1, 3 and 5 days.[19] Three pieces of co-cultured discs for each group were washed twice with PBS, 400 μL DMEM with supplement 40 μL 5 mg mL^{-1} MTT (Amresco, USA) solution was added and incubated at 37 °C for 4 h to form MTT formazan. Finally, the medium was replaced with 400 μL dimethyl sulfoxide (DMSO, Sigma, USA) in order to dissolve the formazan, while the absorbance was measured at 490 nm using an ELX Ultra Microplate Reader (Bio-tek, USA).

Alkaline phosphatase (ALP) activity. The ALP activity was determined as previously described at day 7, 10 and 14 after cell culturing with scaffolds.[19] Briefly, the cells were collected and resuspended in lysis buffer with 0.2% NP-40. Each scaffold was mixed with *p*-nitrophenyl phosphate (*p*NPP, 1 mg mL^{-1}, Sigma, USA) in 1 M diethanolamine buffer and incubated at 37 °C for 15 min. Then, the reaction was stopped by the addition of 3 N NaOH to the reaction mixture. Finally, ALP activity was quantified by ELX Ultra Microplate Reader with absorbance at 405 nm, while total protein content was determined with the Bradford method in aliquots of the same samples with the Bio-Rad protein assay kit (Bio-Rad, USA), read at 630 nm and calculated according to a series of BSA (Sigma, USA) standards. ALP activity was expressed as absorbance at 405 nm (OD value) per milligram of total cellular proteins.

In vivo osteogenesis of scaffolds

Animal surgery. The female New Zealand white rabbit (3 months in age and around 2.8 in weight) were used according to guidelines (NIH guidelines for the care and use of laboratory animals (NIH Publication no. 85-23 Rev. 1985)), which were approved by the Animal Experiment and Care Committee of Ninth People's Hospital affiliated to Shanghai Jiao Tong University School of Medicine. Briefly, the 9 rabbits were randomly divided into 3 groups, and anesthetized with intramuscular injection of sodium pentobarbital (20 mg kg^{-1}, Sigma, USA). Then an incision with length of 1 cm was created to expose the lateral site of right femoral condyle of each rabbit, and a medical high-speed bur was used to drill holes (6 mm in diameter, 6 mm in depth) and C0, C10 and C20 scaffolds were inserted into holes immediately. Subsequently, the incisions were closed with sutures. At week 4 and 12 after surgery, the rabbits in the corresponding group were sacrificed by an overdose of pentobarbital sodium, and the bone samples containing scaffolds were harvested and fixed by 2.5% glutaraldehyde solution.

Micro-computed tomography (m-CT) analysis. The bone samples were examined by a micro-CT system (mCT-80, Scanco Medical AG, Switzerland) with spot size of 20 mm and maximum voltage of 36 kV. After micro-CT scan, the 2D images of all bone samples were integrated by Adobe Photoshop CS6 Software (Adobe System, USA).

Histological analysis. After m-CT evaluation, the bone samples were decalcified using 15% ethylenediaminetetraacetic acid (EDTA, Fluka BioChemika, Sigma-Aldrich), bisected in the longitudinal axis using the lateral border of the intercondylar notch as a guide, and processed using an automated tissue processor (ASP300, Leica, Germany) before being embedded in paraffin wax blocks. Sections (7 μm) were cut using a rotary microtome (Microsystems GmbH, Germany) and mounted on poly-L-lysine coated glass slides (ThermoScientific, Menzel&Co KG, Germany). The sections were then stained using Masson's trichrome staining. The optical microscope was conducted to observe the new bone formation and ingrowth, and the quantitative analysis of new bone, mature bone and material residual were assessed using Image Pro Plus 6.0 software.

Statistical analysis

All data were expressed as means ± SD. Statistical analysis was performed by ANOVA and SNK *post hoc* or Kruskal–Wallis nonparametric procedure followed by Mann–Whitney U test for multiple comparisons based on the normal distribution and equal variance assumption test, using SPSS v.10.1 software (SPSS Inc, USA). Values of $p < 0.05$ were considered statistically significant.

Results

Characterization of n-MS and n-MS/ZN/PCL scaffolds

Fig. 1a shows the TEM image of n-MS particles, which exhibited sphere-like particles with the size of around 200 nm. Fig. 1b shows the EDS patterns of n-MS, the peaks of Mg and Si elements were found. Fig. 1c reveals the XRD patterns of n-MS and ZN, the wide peaks at $2\theta = 20$–$30°$ were found in both n-MS and ZN, indicating amorphous phase. Fig. 2d reveals the XRD patterns of C0, C10 and C20 scaffolds. The characteristic

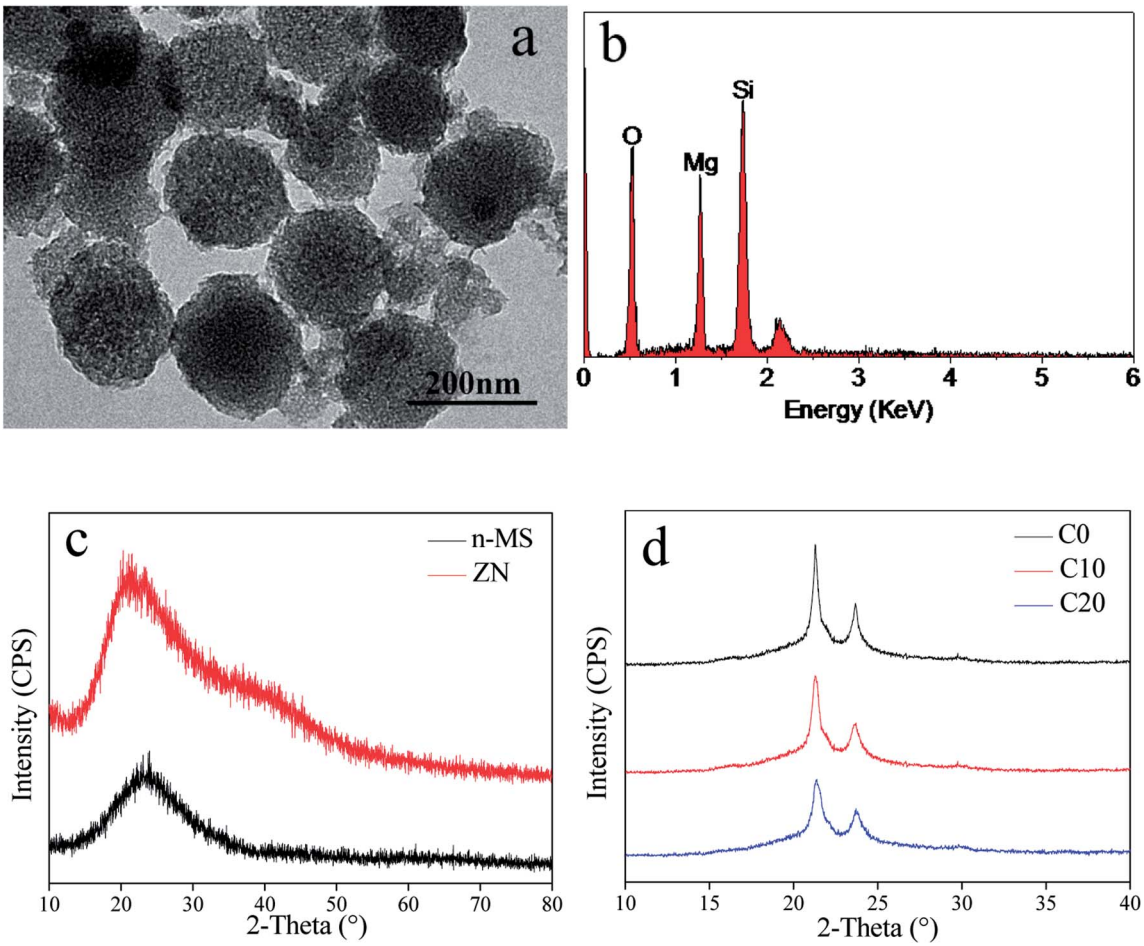

Fig. 1 TEM image (a) and EDS (b) of n-MS, and XRD (c) of n-MS and ZN, and XRD (d) of C0, C10 and C20 scaffolds.

peaks at $2\theta = 21°$ and 23° were ascribed to PCL. In addition, the characteristic peaks of PCL exhibited no obvious change with the increase of ZN content, indicating that incorporation of ZN into PCL had no significant effects on crystallinity of PCL.

The SEM micrographs of surface morphology of C0, C10 and C20 scaffolds are shown in Fig. 2. The scaffolds fabricated by 3D printing technology showed well interconnected macroporous structure and the pores sizes were around 500 μm. The surfaces of macropores walls of the scaffolds became rough with the increase of ZN content. The compressive strength and porosity of the 3D-printed scaffolds were shown in Table 2. It was found that the compressive strength of C0, C10 and C20 scaffolds was 7.1 MPa, 6.8 MPa and 6.5 MPa. Moreover, the porosity of C0, C10 and C20 scaffolds was 71.4%, 71.6% and 72.1%, no obvious difference in porosity for these scaffolds was found.

Apatite-mineralization of scaffolds

As shown in Fig. 3 (a–f), some sphere-like apatite with the size of several micrometers were found to deposit on the surfaces of C0, C10 and C20 scaffolds after immersed into SBF for 5 days. In addition, the amounts of apatite on the C20 scaffolds were more than C10 and C0 scaffolds. The peaks of Ca and P were shown on C20 scaffold by EDS after immersed in SBF for 5 days (Fig. 3g), further confirming that the apatite was deposited on C20 scaffold surface. The ratio of Ca to P of the deposited apatite was 1.62, which was closed to hydroxyapatite of 1.67.[23] The concentration of Ca and P ions gradually decreased with time (Fig. 3h) as the formation of apatite obviously consumed large amounts of Ca and P ions, while the Si and Mg ions concentrations kept increasing because of dissolution of composites scaffolds, which released Si and Mg.

Degradation of scaffolds *in vitro*

The weight loss (degradation) of the scaffolds in PBS increased with time (Fig. 4a). In addition, the weight loss of C20 was significantly higher than C10 and C0 scaffold. The results indicated that the degradability of scaffolds increased with ZN content in the scaffolds (C20 > C10 > C0). The pH values of the PBS solution for both C0 and C10 scaffold obviously increased with time (Fig. 4b), and the increase of pH for C0 was higher than C10 scaffold. However, no obvious change of pH for C20 scaffold during immersing time. At 84 days, the pH values of the solution for C20, C10 and C0 scaffolds were 7.47, 7.71 and 7.83.

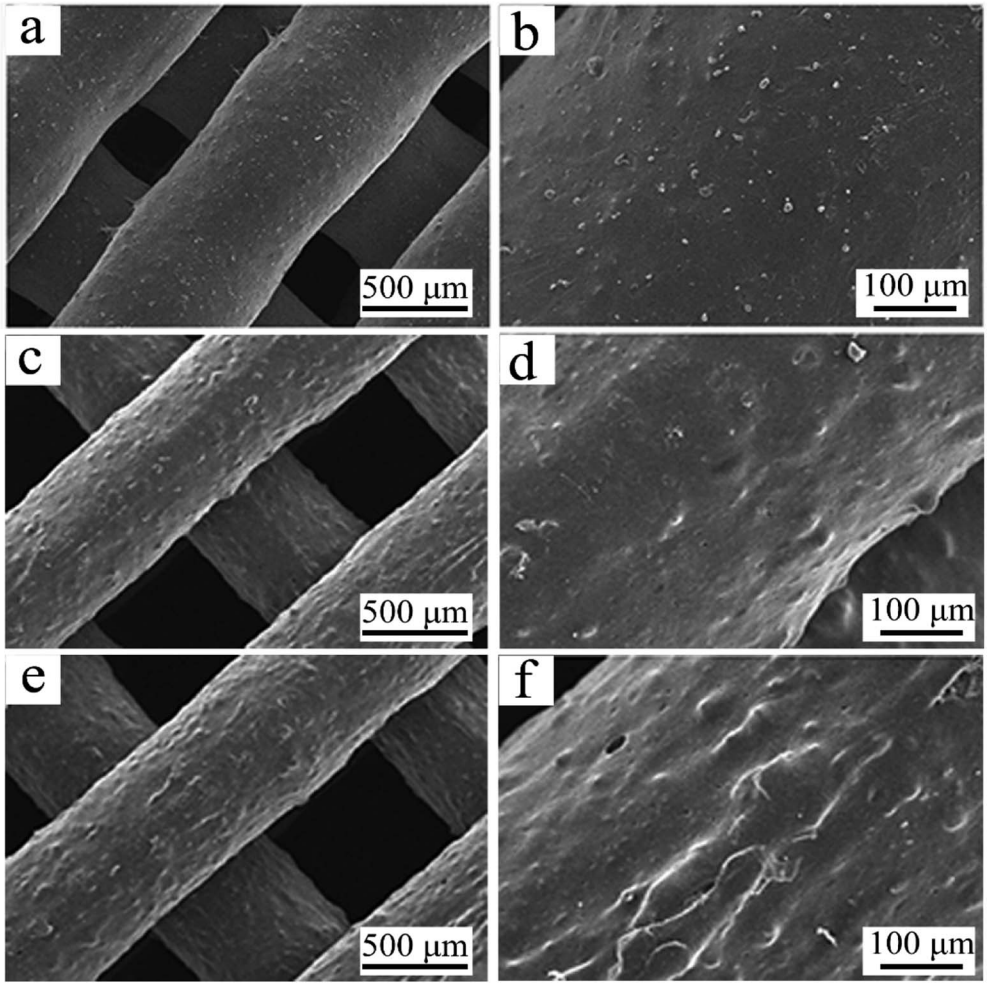

Fig. 2 SEM micrographs of C0 (a and b), C10 (c and d) and C20 (e and f) scaffolds under different magnification.

Table 2 Porosity and compressive strength of 3D-printed scaffolds

Samples	Porosity (%)	Compressive strength (MPa)
C0	71.4 + 3.2	7.1 + 1.8
C10	71.6 + 2.8	6.8 + 2.1
C20	72.1 + 2.3	6.5 + 2.0

Cell morphology, proliferation and ALP activity of cells on scaffolds

The MC3T3-E1 cells were found to grow into macropores of the three kinds of scaffolds as shown in Fig. 5. Moreover, the amounts of the cells on C20 were obviously higher than those of C10 and C0 scaffolds, and C10 was more than C0 scaffold.

Fig. 6a reveals the OD values (cell proliferation) of MC3T3-E1 cells cultured on the scaffolds for 1, 3 and 5 days. The OD values of the cells on the three kind scaffolds increased with the increase of time, indicating that the cells could proliferate with time (good cytocompatibility of the scaffolds). At 1, 3 and 5 days, the OD values for C20 and C10 scaffolds were higher than C0, revealing that C20 and C10 scaffolds containing ZN promoted cells proliferation (no obvious difference between C20 and C10). In addition, at 3 and 5 days, the OD values of cells for C20 scaffold was significantly higher than C10 scaffold, and C10 was higher than C0 scaffold, showing that the OD values of cells increased with the increase of ZN content in scaffolds, and C20 scaffold exhibited the highest ability to promoted cells proliferation. Fig. 6b shows the ALP activity of the cells cultured on the scaffolds for different time. At 7 and 10 day, the ALP activity of the cells for C20 was significantly higher than C10 and C0 scaffolds while no obvious difference for C10 and C0 scaffolds was found, indicating that C20 containing more ZN improved cells differentiation. At 14 days, the ALP activity of the cells for C20 was higher than C10 scaffold, and C10 was higher than C0 scaffold, indicating that ALP activity of cells increased with ZN content in the scaffolds, and C20 possessed the highest ability to promoted cells differentiation.

Osteogenesis of scaffolds *in vivo*

The 2D images from micro-CT after C0, C10 and C20 scaffolds implanted *in vivo* for different time as shown in Fig. 7. It was found that the newly formed bone tissues (NBs) in C0, C10 and C20 scaffolds increased with time. In addition, the amount of

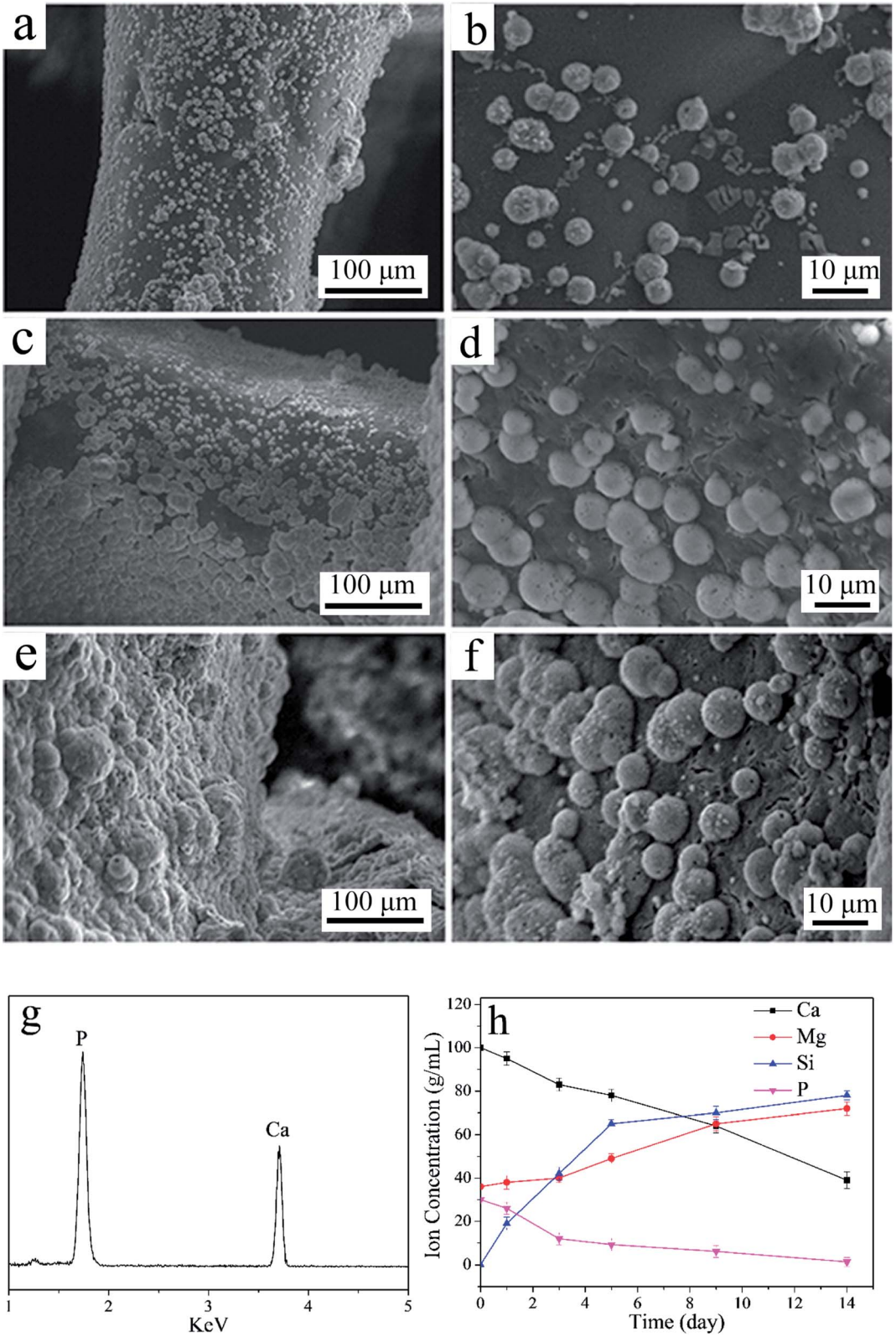

Fig. 3 SEM micrographs of C0 (a and b), C10 (c and d) and C20 (e and f) scaffolds under different magnification after immersed into SBF for 5 days, EDS (g) of C20 scaffold immersed into SBF for 5 days, and the change of ions concentrations with time (h) after C20 scaffold immersed into SBF.

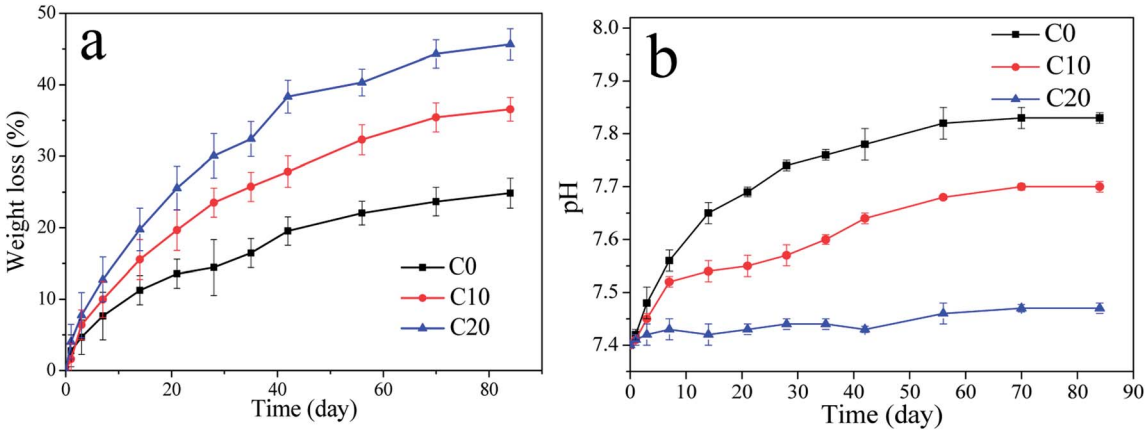

Fig. 4 Weight loss (a) of samples in PBS with time and the change of pH values (b) in solution with time after C0, C10 and C20 scaffolds immersed into PBS.

NBs growth into the scaffolds increased with the increase of ZN content in the scaffolds.

The histological images (Fig. 8A) revealed that the NBs were found to grow into the scaffolds, and the amounts of NBs growth into the scaffolds increased with time. Moreover, the amounts of NBs increased with the increase of ZN content in the scaffolds. The quantitative analysis of NBs area (Fig. 8B) showed that the NBs area for all scaffolds increased with time, and the NBs area increased with the increase of ZN content in the scaffolds. Accordingly, the material residual for all scaffolds decreased with time (Fig. 8C), and the decrease of material residual with the increase of ZN content in the scaffolds.

Discussions

In bone tissue engineering application, concisely control of the architectures of the porous scaffolds (*e.g.* pore size, porosity, pore morphology and pore interconnectivity, *etc.*) would benefit

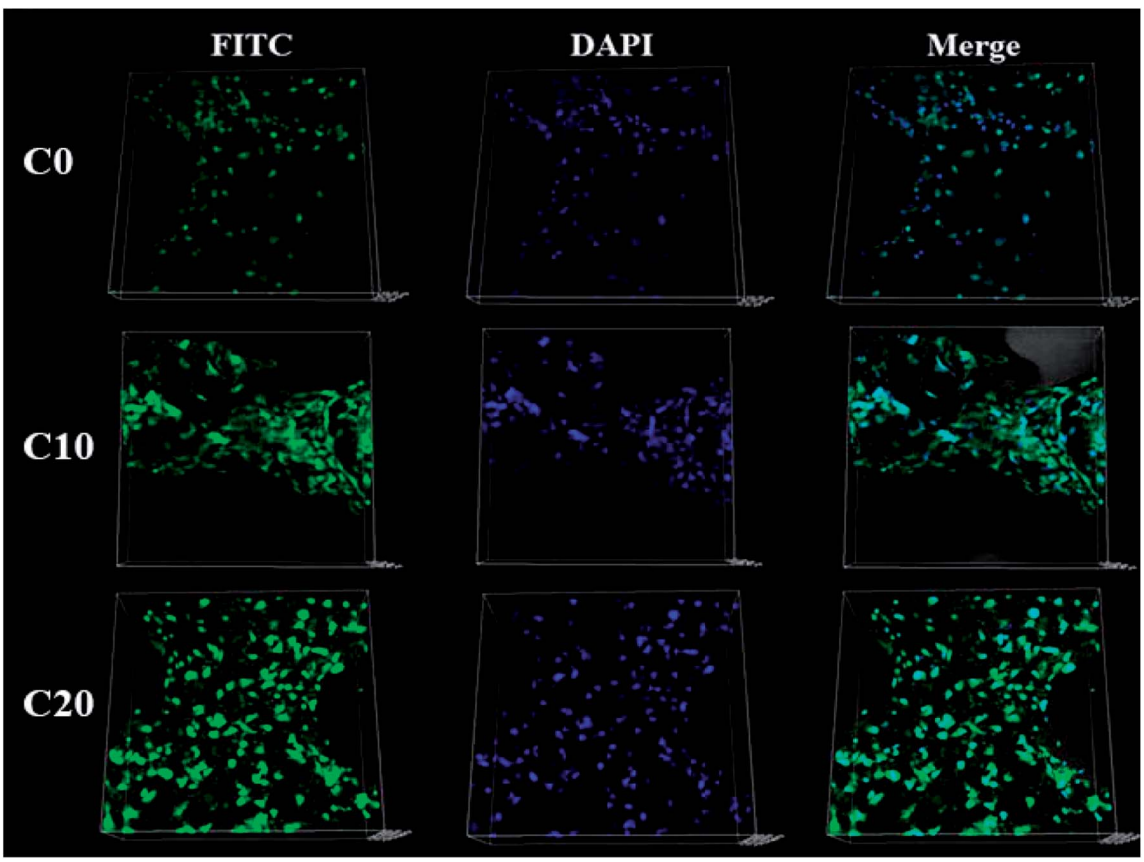

Fig. 5 CLSM images of the MC3T3-E1 cells cultured on C0, C10 and C20 scaffolds for 12 h.

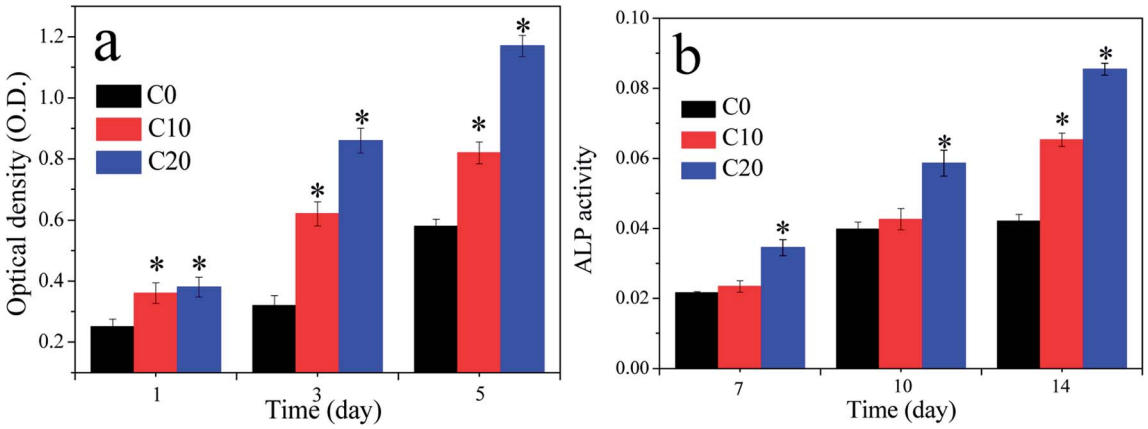

Fig. 6 Optical density (OD) values (a) and ALP activity (b) of the cells cultured on C0, C10 and C20 scaffolds for different time, *$p < 0.05$.

for cells/tissues ingrowth and nutrient delivery.[17,20] In this study, bioactive and degradable scaffolds of n-MS/ZN/PCL ternary composites were developed by using 3D-printing technology. The results showed that the pore morphology, pore interconnection, pore size as well as porosity of the (C0, C10 and C20) scaffolds could be controlled by using 3D-printing technique, and the highly interconnected scaffolds possessed the controllable macropores size of around 500 μm and porosity of around 70%. In addition, compared with C0 without ZN (smooth), the surfaces of macroporous walls of C10 and C20 scaffolds containing ZN became rough. Moreover, no obvious differences in compressive strength of the C0, C10 and C20 scaffolds were found, indicating that the addition of ZN did not obviously affect the compressive strength of the 3D-printed scaffolds.

Apatite mineralization on the biomaterial surface in simulated body fluid (SBF) is a generally accepted way to evaluate the *in vitro* bioactivity, which is also usually utilized to predict the

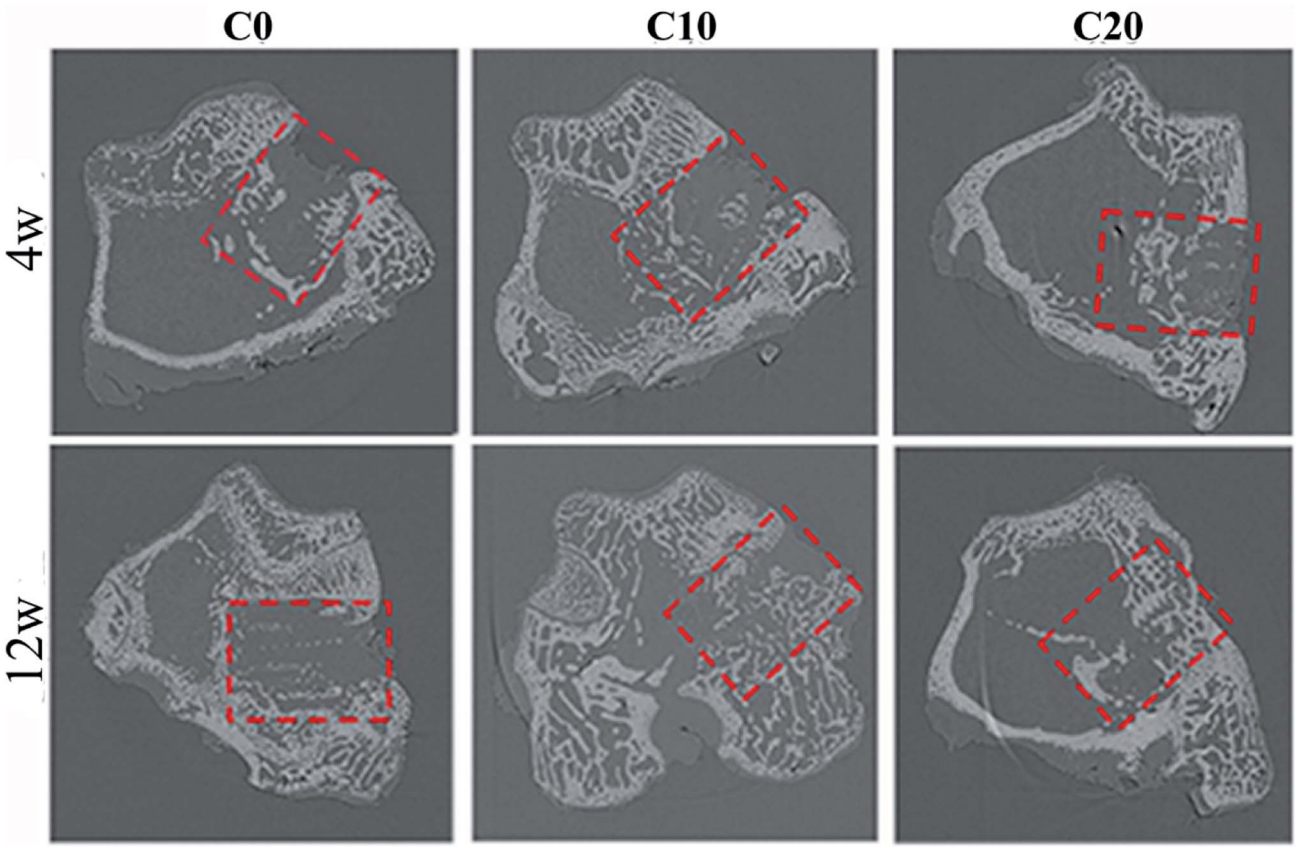

Fig. 7 The 2D images of bone-scaffolds from micro-CT after C0, C10 and C20 scaffolds implanted into femoral defects of rabbits at 4 and 12 weeks.

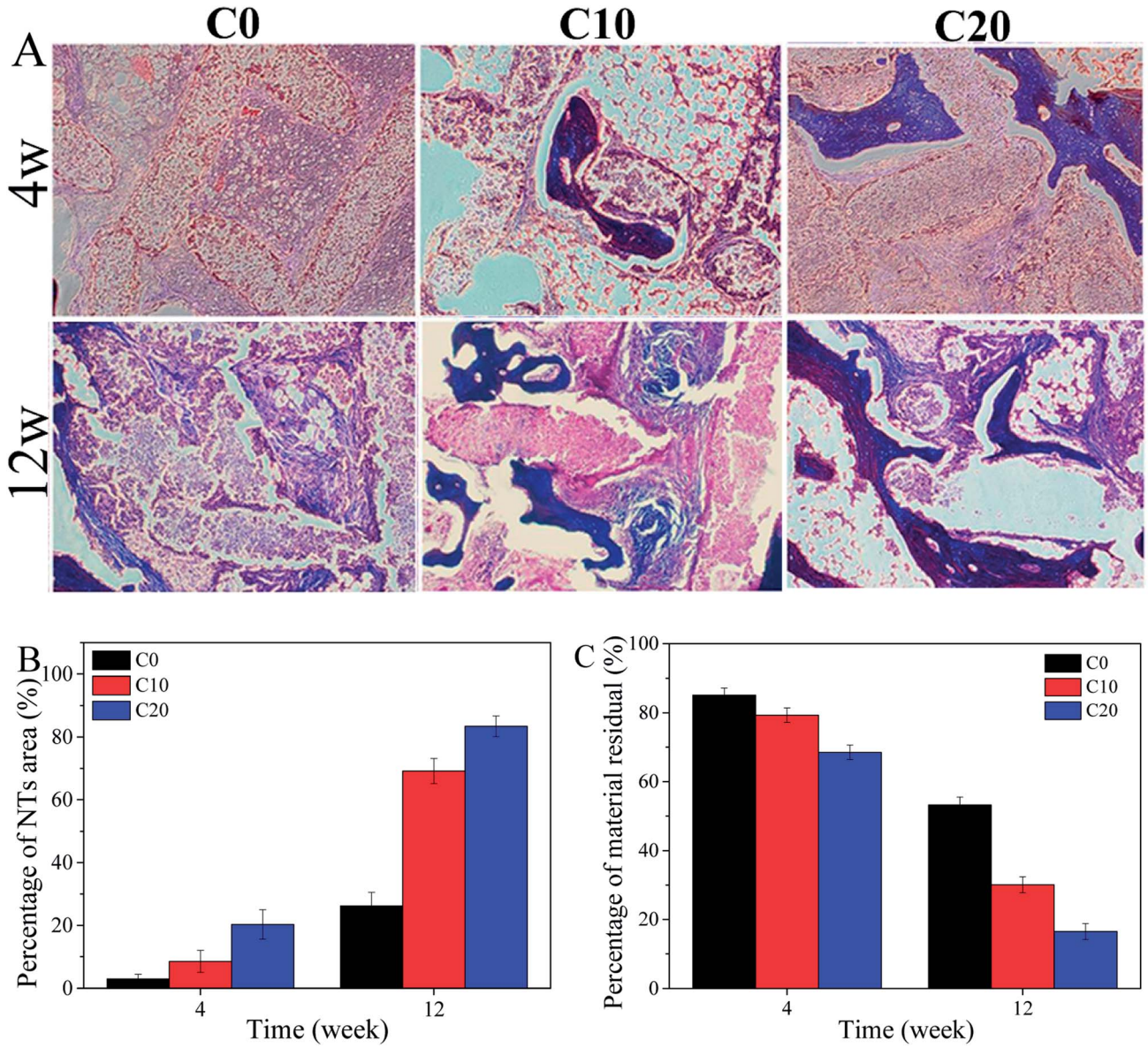

Fig. 8 Images of histological sections (×100, Masson staining) (A), percentage of NBs area (B) and material residual (C) after C0, C10 and C20 scaffolds implanted into femoral defects of rabbits for 4 and 12 weeks.

bioactivity (osteogenic activity) of the biomaterial *in vivo*.[21] In this study, the results suggested that the apatite mineralization ability of the scaffolds increased with the increase of ZN content, indicating that incorporation of ZN into the scaffolds could improve their apatite mineralization ability. The C20 scaffolds exhibited the highest apatite mineralization ability, indicating the best bioactivity.[22] The mechanism of apatite mineralization on the scaffolds was due to the presence of n-MS, which was similar to the apatite mineralization on n-MS as previous publications.[23] Moreover, it can be suggested that the first degradation of ZN (due to fast degradation rate of ZN) might improve the surface area of the scaffolds with more n-MS exposing on their surfaces, which further promoted the apatite mineralization.[24] Furthermore, the first degradation of ZN as well as n-MS particles exposing on the macroporous walls formed rough surfaces on the scaffolds that might offer more nucleation sites for apatite mineralization.[25] The C20 containing more amounts of ZN than C10 scaffold. Therefore, the C20 scaffold exhibited the highest apatite mineralization ability.

Ideal scaffolds for bone tissue engineering should possess the matched speed of degradation with the formation of new bone when implanted *in vivo*.[26] In this study, the results showed that incorporation of ZN into the scaffolds was conducive to improve their degradability (increased with the increase of ZN content), in which C20 scaffold possessed the fastest degradation rate. It can be suggested that the first degradation of ZN might form some micropores on the surfaces of the scaffold, which increased the surface area of the scaffolds.[27] Therefore, incorporation of ZN promoted the degradation of the scaffold, which increased with the increase of ZN content. The pH values

in PBS for both C0 and C10 obviously increased with time while no obvious change for C20 scaffolds. The increase of pH for C0 in PBS was due to the degradation of n-MS in the scaffolds, which produced alkaline products, and formed alkaline micro-environment (micro-environment too alkaline to cells growth).[28] However, the degradation of ZN in both C10 and C20 produce acidic products (*e.g.* amino acid),[29] which would neutralize the alkaline products from the degradation of n-MS. The amounts of ZN in C20 were more than C10, which would produce more acidic products (neutralize the alkaline products from n-MS), and formed a micro-environment of pH value (7.47) similar to biological environment. Thus C20 scaffolds showed no change of pH value compared with initial value. The results indicated that incorporation of ZN into the scaffolds could regulate the local pH value in degradable solution, which could avoid too high pH to cells growth.[30]

Ideal scaffolds for bone regeneration should be able to stimulate cells proliferation, which is closely associated with new bone formation *in vivo*.[31] The results in the present study verified that the proliferation of MC3T3-E1 cells on the scaffolds significantly enhanced with the increase of ZN content, and C20 scaffold exhibited the highest ability to promoted cells proliferation. In addition, the results from CLSM images indicated that the cells grew into the scaffolds, and the amounts of the cells in C20 scaffold were more than C10 and C0 scaffolds, indicating that the C20 scaffolds not only stimulated cells proliferation but also promoted cells growth into the scaffolds.[19] ALP activity is generally regarded as an early marker of the differentiation of osteoblasts, and an indicator of osteogenesis *in vivo*.[32] The present study showed that the ALP activity of cells on C20 was obviously higher than C10 scaffolds, and C10 was higher than C0 scaffolds. It could be suggested that the amounts of ZN in the scaffolds had obvious effects on ALP activity of cells. Overall, the C20 scaffolds significantly promoted cell proliferation and osteogenic differentiation, indicating good cytocompatibility.[19]

Previous studies have shown that the release of ions (*e.g.* Si, Mg, *etc.*) from bioactive scaffolds was a key factor that influenced the cell responses (*e.g.* cells proliferation and differentiation, *etc.*).[33] In this study, the Si and Mg ions were found to release from C20 scaffold into SBF due to the dissolution of n-MS in the scaffold. Therefore, the improvements of cell proliferation and ALP activity of MC3T3-E1 cells were attributed to the release of these ions from the scaffolds. Moreover, the first degradation of ZN in C20 would lead to further degradation of n-MS (surface area of C20 increase), which released more Si and Mg ions (C20 > C10) in the micro-environment to stimulate cells responses.[24] In addition, the formation of rough surface of the C20 scaffold due to the increase of ZN content (compared with C10 and C0) might be useful for the cells responses (*e.g.* cell adhesion).[34] Furthermore, the formation of apatite on the scaffolds might stimulate the cells responses (*e.g.* cell differentiation).[35]

As a scaffold for bone regeneration, it is critical to investigate its osteogenic ability *in vivo* using animal models.[36] In the present study, the osteogenic ability of the scaffolds implanted *in vivo* was studied by micro-CT and histological analysis. The results confirmed that the newly formed bone tissues (NBs) in the scaffolds increased with the increase of ZN content, and C20 possessed the best osteogenic ability, indicating that ZN played key roles on improvement the osteogenic ability of the scaffolds. In addition, the histological images and quantitative analysis demonstrated that the NBs grew into the scaffolds, and the amounts of NBs increased with the increase of ZN content, in which the C20 possessed the highest new bone formation ability. Accordingly, the material residual for the scaffolds decreased with the increase of ZN content, and C20 exhibited the lowest material residual, indicating good degradability. The mechanism of degradation of scaffolds *in vivo* was different from *in vitro*. The mechanism of degradation of scaffolds *in vitro* was the dissolution. However, the mechanism of degradation of scaffolds *in vivo* included two factor: dissolution and cell-mediated degradation (biodegradation).[37] It could be suggested that incorporation of ZN into scaffolds not only significantly improved the osteogenic ability but also promoted the degradability of the scaffolds *in vivo*.[38]

The generally accepted mechanism of new bone formation in the bioactive scaffold assumed that osteoblasts first adhered to the scaffold surface, formed bone matrix, then mineralized to form bone tissues.[39] The process of bone formation was favored by the apatite-mineralization on the scaffold in a physiological environment because the mineralized apatite (closely resembles bone mineral in composition and structure) might serve as a foundation for osteogenesis.[40] In this study, apatite-mineralization ability of the scaffolds increased with the ZN content, and C20 scaffold exhibited the highest apatite-mineralization ability. Therefore, the improvement of new bone formation ability for C20 scaffold was ascribed to the enhancement of apatite-mineralization ability of the scaffold, which increased with ZN content. In addition, previous studies have revealed that the Mg and Si ions release from bioglass/ceramics could not only stimulate the proliferation and differentiation of osteoblasts and hBMSCs *in vitro* but also promoted new bone formation *in vivo*.[41] Therefore, the enhancement of osteogenesis of C20 *in vivo* might be attributed to the release of Mg and Si ions from the scaffolds. In summary, the *in vitro* and *in vivo* results indicated that the excellent biocompatibility, degradability and osteogenesis of the scaffolds of n-MS/ZN/PCL ternary composites were attributed to the bioperformances of both the n-MS and ZN together in the scaffolds, and the addition of ZN into the scaffolds might be an effective strategy to improve the bioperformance of 3D-printed scaffolds.

Conclusions

Bioactive and degradable scaffolds of n-MS/ZN/PCL ternary composites were developed by 3D-printing method for bone tissue engineering applications. The results showed that the scaffolds possessed well interconnected macropores of around 500 μm and controllable porous structures. The *in vitro* apatite mineralization ability and degradability of the scaffolds were greatly improved with the increase of ZN content, in which C20 scaffold possessed the highest apatite mineralization ability and the fastest degradability. The scaffolds containing ZN

significantly promoted the proliferation and early differentiation of MC3T3-E1 cells, which depended on the content of ZN. Furthermore, the *in vivo* osteogenesis of the 3D-printed scaffolds was obviously enhanced, which depended on the content of ZN. The results demonstrated that the ternary composites scaffolds combined with advantages of both n-MS and ZN could effectively promote bone regeneration. The C20 scaffold prepared by the 3D-printing method had a great potential for bone tissue engineering applications.

Conflicts of interest

There are no conflicts to declare.

Acknowledgements

The grants were from the National Natural Science Foundation of China (81772343), and the Research Project of Jiangsu Provincial Health and Family Planning Commission (H201662).

Notes and references

1 J. Zhang, S. Zhao, Y. Zhu, Y. Huang, M. Zhu, C. Tao and C. Zhang, *Acta Biomater.*, 2014, **10**, 2269–2281.
2 C. M. Curtin, G. M. Cunniffe, F. G. Lyons, K. Bessho, G. R. Dickson, G. P. Duffy and F. J. O'Brien, *Adv. Mater.*, 2012, **24**, 749–754.
3 S. Sprio, A. Tampieri, G. Celotti and E. Landi, *J. Mech. Behav. Biomed. Mater.*, 2009, **2**, 147–155.
4 Q. Fu, M. N. Rahaman, B. S. Bal, R. F. Brown and D. E. Day, *Acta Biomater.*, 2008, **4**, 1854–1864.
5 J. A. Sowjanya, J. Singh, T. Mohita, S. Sarvanan, A. Moorthi, N. Srinivasan and N. Selvamuruqan, *Colloids Surf., B*, 2013, **4**, 294–300.
6 T. Qu and X. Liu, *J. Mater. Chem. B*, 2013, **1**, 4764–4772.
7 C. Isikli, V. Hasirci and N. Hasirci, *J. Tissue Eng. Regener. Med.*, 2012, **6**, 135–143.
8 H. T. Oyama, D. Tanishima and S. Maekawa, *Polym. Degrad. Stab.*, 2016, **134**, 265–271.
9 E. J. Chong, T. T. Phan, I. J. Lim, Y. Z. Zhang, B. H. Bay, S. Ramakrishna and C. T. Lim, *Acta Biomater.*, 2007, **3**, 321–330.
10 F. Wu, J. Wei, C. S. Liu, B. O'Neil and Y. Ngothai, *Composites, Part B*, 2012, **43**, 2192–2197.
11 Y. Miao, R. Yang, D. Y. B. Deng and L. M. Zhang, *RSC Adv.*, 2017, **7**, 17711–17719.
12 E. Corradini, P. S. Curti, A. B. Meniqueti, A. F. Martins, A. F. Rubira and E. C. Muniz, *Int. J. Mol. Sci.*, 2014, **15**, 22438–22470.
13 M. Demir, L. Ramos-Rivera, R. Silva, S. N. Nazhat and A. R. Boccaccini, *J. Biomed. Mater. Res., Part A*, 2017, **105**, 1656–1665.
14 S. Babitha and P. S. Korrapati, *Biomed. Mater.*, 2017, **12**, 055008.
15 Y. Zhang, N. Cheng, R. Miron, B. Shi and X. Cheng, *Biomaterials*, 2012, **33**, 6698–6708.
16 B. Rais, M. Koster, M. I. Rahim, M. Pils, J. M. Seitz, H. Hauser, D. Wirth and P. P. Mueller, *J. Biomed. Mater. Res., Part A*, 2016, **104**, 2149–2158.
17 C. H. Zhang, D. Cheng, T. H. Tang, X. L. Jia, Q. Cai and X. P. Yang, *J. Mater. Chem. B*, 2015, **3**, 5300–5309.
18 C. Kascholke, S. Hendrikx, T. Flath, D. Kuzmenka, H. M. Dorfler, D. Schumann, M. Gressenbuch, F. P. Schulze, M. Schulz-Siegmund and M. C. Hacker, *Acta Biomater.*, 2017, **63**, 336–349.
19 Y. L. Li, Y. Xiao and C. S. Liu, *Chem. Rev.*, 2017, **117**, 4376–4421.
20 J. A. Inzana, D. Olvera, S. M. Fuller, J. P. Kelly, O. A. Graeve, E. M. Schwarz, S. L. Kates and H. A. Awad, *Biomaterials*, 2014, **35**, 4026–4034.
21 A. M. Deliormanli and M. N. Rahaman, *J. Eur. Ceram. Soc.*, 2012, **32**, 3637–3646.
22 A. Rifai, N. Tran, D. W. Lau, A. Elboutne, H. L. Zhan, A. D. Stacey, E. L. H. Mayes, A. Sarker, E. P. Ivanova, R. J. Crawford, P. A. Tram, B. C. Gibson, A. D. Greentree, E. Pirogova and K. Fox, *ACS Appl. Mater. Interfaces*, 2018, **10**, 8474–8484.
23 T. W. Sun, W. L. Yu, Y. J. Zhu, R. L. Yang, Y. Q. Shen, D. Y. Chen, Y. H. He and F. Chen, *ACS Appl. Mater. Interfaces*, 2017, **9**, 16435–16447.
24 Z. R. Gu, S. C. Wang, W. Z. Weng, X. Chen, L. H. Cao, J. Wei, J. W. Shin and J. C. Su, *Mater. Sci. Eng., C*, 2017, **75**, 620–628.
25 Z. Y. Wu, Q. Li, Y. K. Pan, Y. Yao, S. C. Tang, J. C. Su, J. W. Shin, J. Wei and J. Zhao, *Int. J. Nanomed.*, 2017, **12**, 3637–3651.
26 L. Krishnan, L. B. Priddy and C. Esancy, *Acta Biomater.*, 2016, **49**, 101–112.
27 Z. Fereshteh, M. Fathi, A. Bagri and A. R. Boccaccini, *Mater. Sci. Eng., C*, 2016, **68**, 613–622.
28 Z. Y. Wu, K. Zheng, J. Zhang, T. T. Tang, H. Guo, A. R. Boccaccini and J. Wei, *J. Mater. Chem. B*, 2016, **4**, 7974–7988.
29 X. Chen, D. S. Brauer, N. Karpukhina, R. D. Waite, M. Barry, I. J. Mckay and R. G. Hill, *Mater. Lett.*, 2014, **126**, 278–280.
30 H. J. Wang, S. J. Gong, Z. X. Lin, J. X. Fu, S. T. Xue, J. C. Huang and J. Y. Wang, *Biomaterials*, 2007, **28**, 3952–3964.
31 E. Ko, K. Yang, J. Shin and S. W. Cho, *Biomacromolecules*, 2013, **14**, 3202–3213.
32 H. M. Zhang, J. H. Wang, F. Deng, E. Y. Huang, Z. J. Yan, Z. L. Wang, Y. L. Deng, Q. Zhang, Z. L. Zhang, J. X. Ye, M. Qiao, R. F. Li, J. Wang, Q. Wei, G. L. Zhou, H. H. Lu, R. C. Haydon, T. C. He and F. Deng, *Biomaterials*, 2015, **39**, 145–154.
33 C. T. Wu, R. Miron, A. Sculean, S. Kaskel, T. Doert, R. Schulze and Y. F. Zhang, *Biomaterials*, 2011, **32**, 7068–7078.
34 L. Cai, Y. K. Pan, S. C. Tang, Q. Li, T. T. Tang, K. Zheng, A. R. Boccaccini, S. C. Wei, J. Wei and J. C. Su, *J. Mater. Chem. B*, 2017, **5**, 8337–8352.
35 G. Pezzotti, N. Oba, W. L. Zhu, E. Marin, A. Rondinella, F. Boschetto, B. McEntire, K. Yamamoto and B. S. Bal, *Acta Biomater.*, 2017, **64**, 411–420.

36 Q. Q. Yao, J. G. L. Cosme, T. Xu, J. M. Miszuk, P. H. S. Picciani, H. Fong and H. L. Sun, *Biomaterials*, 2017, **115**, 115–127.
37 A. J. Drelich, S. Zhao, R. J. Guillory, J. W. Drelich and J. Goldman, *Acta Biomater.*, 2017, **58**, 539–549.
38 P. Y. Zhou, Y. Xia, X. S. Cheng, P. F. Wang, Y. Xie and S. G. Xu, *Biomaterials*, 2014, **35**, 10033–10045.
39 S. Cao, H. J. Li, K. Z. Li, J. H. Lu and L. L. Zhang, *J. Biomed. Mater. Res., Part A*, 2016, **104**, 533–543.
40 M. C. Xu, D. Zhai, J. Chang and C. T. Wu, *Acta Biomater.*, 2014, **10**, 463–476.
41 M. C. Tousi, M. F. Velten, T. J. Bishop, K. K. Leong, N. S. Barkhordar, G. W. Marshall, P. M. Loomer, P. B. Aswath and V. G. Varanasi, *Mater. Sci. Eng., C*, 2013, **33**, 2757–2765.